Published in final edited form as:
Neuron. 2009 February 12; 61(3): 397–411. doi:10.1016/j.neuron.2008.12.024.

Two Pathways of Synaptic Vesicle Retrieval Revealed by Single Vesicle Imaging

Yongling Zhu*, **Jian Xu**, and **Stephen F. Heinemann**
Molecular Neurobiology Laboratory, The Salk Institute, 10010 North Torrey Pines Rd, La Jolla, CA 92037

Summary

Synaptic vesicle recycling is essential for maintaining efficient synaptic transmission. Detailed dissection of single vesicle recycling still remains a major challenge. We have developed a new fluorescent pH reporter that permits us to follow the fate of individual vesicles at hippocampal synapses after exocytosis. Here we show that, during low frequency stimulation, single vesicle fusion leads to two distinct vesicle internalizations, instead of one, as in general perception: one by a fast endocytosis pathway (~3s), the other by a slow endocytosis pathway (after 10s). The exocytosed vesicular proteins are preferentially recaptured in both pathways. RNAi knocking down of clathrin inhibits both pathways. As stimulation frequency increases, the number of endocytosed vesicles begins to match antecedent exocytosis. Meanwhile, the slow endocytosis is accelerated and becomes the predominant pathway. These results reveal that two pathways of endocytosis are orchestrated during neuronal activity, enabling the highly efficient endocytosis machinery at central synapses.

Introduction

At nerve terminals, neurotransmitter release is mediated by exocytosis of synaptic vesicles at active zone. After exocytosis, vesicular components are efficiently retrieved by endocytosis to sustain the synaptic transmission over time. Although synaptic vesicle recycling has been extensively studied, an understanding of the basic steps of this process is still lacking, in part because it has been difficult to study the behavior of individual vesicles. For example, it is still debated whether synaptic vesicles are refilled and reused after releasing the contents of their lumen (Aravanis et al., 2003; Klingauf et al., 1998; Murthy and Stevens, 1998; Pyle et al., 2000; Richards et al., 2000a) or are reconstituted anew (Li et al., 2005; Richards et al., 2000b; Takei et al., 1996; Zenisek et al., 2002). Further, if the vesicle membrane is reused, it is not known if it retains its original synaptic vesicle proteins (Fesce et al., 1994; Gandhi and Stevens, 2003; Willig et al., 2006) or if others are substituted by diffusional exchange while the vesicle is associated with the surface membrane (Fernandez-Alfonso et al., 2006; Wienisch and Klingauf, 2006). The pathways followed in the reclamation of the membrane for a vesicle, and the time occupied by each step, are still uncertain.

The principle behind the method we use is based on the fact that synaptic vesicles maintain their lumen at a pH more acid than the cytoplasm, and that this pH gradient collapses when

Correspondence: yzhu@salk.edu (Y.Z.).

the vesicle interior communicates with the neutral extracellular medium after fusion. We have developed an improved fluorescent reporter of intravesicular pH, based on the approach of Miesenbock et al. (Miesenbock et al., 1998), that provides a signal-to-noise ratio sufficient to address the questions outlined above with high temporal and spatial resolution for single vesicles. The idea is to include four copies of phluorin in an intravesicular loop of the vesicle protein synaptophysin. Because this protein is present in the vesicle membrane with a high copy number (Takamori et al., 2006) and appears not to be required for normal vesicle trafficking (McMahon et al., 1996; Sudhof et al., 1987), we can follow the time course of vesicle acidification and thus infer, from the fluorescence intensity of the phluorin reporters, the behavior of vesicle from fusion pore opening until reacidification.

Unexpectedly, we observed that, after single vesicle fusion, the fluorescence was quenched in two distinct steps. On the basis of experiments described later, we interpret these steps as two distinct vesicles being internalized by kinetically separate endocytic pathways. Thus, exocytosis-endocytosis coupling breaks down at low stimulation frequencies. Interestingly, the tight coupling between exocytosis and endocytosis is reestablished when stimulation frequency increases and multiple vesicles are released. We further characterized the properties of these two separate pathways by their activity-dependence and their molecular identity. We found both pathways were inhibited by clathrin RNAi knocking down. Moreover, we demonstrated that neuron activity affects the usage of two endocytosis pathways. Increasing stimulation intensity or Ca^{2+} influx selectively accelerated the speed of slow endocytosis, without affecting the fast endocytosis. Thus, Ca^{2+} might serve as the initiator for an activity-dependent switch between different mechanisms of synaptic vesicle recycling. Our study suggests that two pathways of endocytosis operate coordinately during neuron activity to establish the highly efficient endocytosis machinery at central synapses.

Results

The Properties of SypHluorins

The reporters we have developed – named ‘SypHluorins’ – consist of one to four pHluorins incorporated into the second intravesicular loop of synaptophysin (Figure 1B). Using the calcium phosphate method to introduce the SypHluorin DNA into cultured hippocampal neurons, we find – based on averages across 138 to 168 synapses –consistent labeling of vesicles with about three-fold less background fluorescence than seen with a similar construct based on VAMP (Synaptobrevin) (Figure 1A). As is clear from Figure 1C, the fluorescence signal-background ratio (averaged across 109 to 196 synapses) produced by a standard stimulus (20 Hz field stimulation for two seconds) is larger when more pHluorins are present in the intravesicular loop, and the four-pHluorin construct based on synaptophysin gives about 6-fold signal-to-background ratio as one based on VAMP (Table 1).

Our first concern was to determine if basal synaptic function is altered by the presence of the labeled synaptophysins. We used the destaining rate averaged across 194 control and 236 SypHluorin (4x) expressing synapses preloaded with FM4-64 as a measure of basal release properties; as is clear from Figure 1D, vesicle fusion rates were not detectably different from control when 4 pHluorins are present per synaptophysin.

To determine the pHluorin bleaching rate under our conditions, we measured the bouton background fluorescence (under constant illumination) as a function of time in 7 experiments (130 boutons). If we assume a single exponential bleaching process, we find the time constant is 3.5 minutes.

Our next concern was to determine if we could detect the fluorescence signal from individual vesicles. Figure 1E presents fluorescence intensity of an imaged bouton as a function of time when single stimuli were presented at 0.2 Hz. This stimulus usually release either zero or one vesicle per bouton, and rapid increases in fluorescence of about the same amplitude appeared after some of the stimulus presentations: three of the ten stimuli gave fluorescence increases of about 200 units, one gave a response of about 400 units, and 6 gave failures of response. In Figure 1F, we present a histogram based on the amplitudes of 505 fluorescence responses to single stimuli from 28 synapses, with a fit of what is expected for a baseline noise standard deviation of 39.3 fluorescence units, and mean single vesicle fluorescence of 196.9 units with a standard deviation of 58.2 units. We conclude that the signal to noise ratio for single vesicle detection is about 5 and that the variability in expression of the reporter from one vesicle to the next is at most 30% (coefficient of variation for vesicle fluorescence on exposure to pH 7.3).

Time Course of Vesicle Fluorescence

Our major goal is to follow the fluorescence intensity change after single exocytic event in order to determine the time course of the vesicle's fate. To our surprise, on more than 85% of the fusion events, single vesicle fluorescence intensity decayed after stimulation in two distinct phases (Figure 2A). Immediately after fusion pore opening, the fluorescence increased rapidly (instantly on our time scale with a 30 Hz image acquisition rate) to about 210 units (213 ± 5), and remained at the maximal value for about 3 seconds (2.9 ± 0.2); we call this the 'initial state' and show the distribution of initial state dwell times in Figure. 2D. Fluorescence intensity then decreased with a time constant of about 3 seconds (Figure 2G) to about half of the initial value (98 ± 5); we designate this as the 'plateau state'. The vesicle fluorescence remained at this plateau state for a minimum of 8 seconds, but usually for more than 15 seconds (18.2 ± 0.6), and then decayed, again with a time constant of about 3 seconds (Figure 2H), back to the base line. The distribution of total dwell times from the initial opening of the fusion pore to the end of the plateau state is presented in Figure 2E; note that the long-time tail of this histogram is attenuated because a smaller number of observations continued past the 25 second time period in some of the recordings. The overall distribution of times from fusion pore opening to the end of both states (Figure 2F) was revealed by combining the dwell times in Figure 2D and Figure 2E.

SypHluorins exhibited steady fluorescence in both low pH (pH 5.6) and high pH (pH 7.3) environments (Supplementary Figure 2), suggesting the fluorescence change after single vesicle fusion resulted from a loss of proteins from the bouton surface. To determine if the time constant for the decrease of vesicle fluorescence reflected the lateral diffusion of reporters out of the bouton, we reanalyzed the vesicle fluorescence intensity from a larger region including the bouton and surrounding axon (Figure 3A). Fluorescence decay of the small region (bouton alone) and large region (bouton plus axon) were almost identical, indicating that there was no diffusional loss of reporters from the bouton after single vesicle fusion. Meanwhile, if the fluorescence decay was caused by reacidification, then it should be prevented by proton pump inhibitors. To test this prediction, we applied V-ATPase inhibitor bafilomycin to block the reacidification of endocytosed vesicles. As shown in Figure 3B, fluorescence intensity decay after single exocytic event was completely blocked by 1 μM bafilomycin in the extracellular medium. Thus, both phases of fluorescence decay reflect internalization and subsequent acidification of reporters, instead of diffusional loss of reporters along the axon.

The classical model of synaptic vesicle recycling involves fusion of the retrieved vesicle with endosome-like compartments before budding of new vesicles from it (Heuser and Reese, 1973). This model may explain our observation of two-step decay. For instance, the first decay of fluorescence may reflect the fusion of retrieved reporters with endosome-like

compartments and subsequent half-acidification due to the intermediate pH (6.0–6.5) inside endosome, whereas the second decay may results from budding of new vesicle from endosome-like compartments and its final acidification by vesicular proton pump. If this model is correct, fluorescence during 'plateau state' should originate from half-quenched proteins inside endosome-like compartments, thus, should not be quenched by extracellular acidification, if we assume extracellular H^+ ions cannot enter the intracellular space. To show that transiently decreasing the extracellular pH does not alter the intracellular pH detectably, we expressed synaptophysin linked to a phluorin reporter on the intracellular C-terminal tail (Figure 3C left). This construct is expressed on surface membrane and vesicle membrane with the pHluorin exposed to the cytoplasm. Its fluorescence at rest is unquenched because the cytoplasmic environment, unlike the vesicle interior, is insufficiently acidic to quench the reporter fluorescence. When the extracellular pH was reduced from 7.3 to 5.6, this reporter remained unquenched (average of 155 synapses; Figure 3C right), thus establishing that a transient extracellular acidification does not appreciably acidify the cytoplamsic environment. We then stimulated a population of synapses expressing our usual SypHluorin reporter construct and found, on averaging across 47 synapses, that extracellular acidification rapidly quenched the plateau fluorescence (Figure 3D right). Thus, the fluorescence during plateau state originate from the unquenched reporters remaining in communication with the extracellular environment, instead of the half-quenched reporters momentarily sorted to intermediate compartments.

FM 1-43 Labeling Reveals Two Distinct Vesicles Retrieved

From the earlier analysis we know both phases of fluorescence decay reflect internalization and subsequent acidification of reporters. But, how could acidification behave in a "two-phase" pattern? One interpretation is that one internalization event proceeds in two distinct steps: the vesicle's fusion pore remains open for about three seconds, and then closes while the vesicle remains attached to the membrane. As the vesicle attempts to reacidify, it is leaking hydrogen ions through an imperfectly closed fusion pore, which leads to the half quenching of fluorescence intensity during 'plateau state'. After a minimum of about ten seconds, but generally much longer, the fluorescence is completely quenched by acidification of the vesicle's lumen after the complete closure of the fusion pore. Alternatively, another logical interpretation is that two distinct internalization events work in series at different times: one at the end of the initial state (~3s), the other at the end of the plateau state (at least 10 s), with each followed by its own reacidification.

To test these two hypotheses, we decided to measure the number of vesicles internalized during the 'initial state' and 'plateau state' by using styryl dye FM 1-43. If there is only one internalization event which proceeds in two distinct steps, as proposed by the first hypotheses, we should see no FM dye labeled vesicle at the end of the 'initial state'. Instead, we should see one FM dye labeled vesicle at the end of the 'plateau state'. This is because, if a leaky fusion pore is present during the 'plateau state', the dye inside the vesicle will either diffuse out laterally (for a lipid fusion pore), or dissociate into the external medium (for a protein fusion pore) upon washing away FM dye from the bath solution. On the other hand, if two distinct internalizations were to complete at different times, we should see one FM dye labeled vesicle at the end of the 'initial state', two labeled vesicles at the end of the 'plateau state'.

In order to estimate the number of FM dye labeled vesicles, we need to calibrate the fluorescence intensity of a single vesicle, as previously described (Murthy and Stevens, 1998). Figure 4A shows the distribution of fluorescence intensity for 761 synaptic boutons after stimulation with 5 action potentials at 1Hz, in the presence of 10μM FM1-43 for 10s. The fluorescence intensity distribution has evenly spaced peaks at integral multiple of 451 units, which we interpret as corresponding to the fluorescence of a single labeled vesicle.

Having estimated the fluorescence intensity of a single vesicle, we turned our attention to test the two hypotheses described above. We stimulated the synaptic boutons in the presence of 10μM FM 1-43 with a single stimulus, and then removed the dye from the surface membrane and external medium at the end of either 'initial state' (~ 6s) or 'plateau state' (~25 s). Given the release probability of 0.387 for individual synapses that we had measured by SypHluorin (data not shown), about 40 % of the boutons were expected to undergo exocytosis after single action potential. If only one internalization event was to complete by the end of the 'plateau state', the 6s dye exposure should not lead to significant labeling at each bouton. On the other hand, if one internalization completes at the end of the 'initial state' and another completes at the end of the 'plateau state', about 40% of boutons is expected to be labeled with FM 1-43 during 6s dye exposure. In fact, in 1034 synaptic boutons from 8 experiments, after expose to dye for 6s, the fluorescence intensity distribution revealed that 49.6% of the boutons were labeled with FM 1-43 and formed a peak centered at 435 units that corresponds to the single vesicle fluorescence. The rest of the boutons didn't uptake any FM 1-43, shown as a peak around 0 (Figure 4C). This observation strongly suggests that, after a single exocytosis, one intact internalization event has completed by the end of the 'initial state'.

In the next experiment, we prolonged the dye exposure to the end of the 'plateau state' (~25s). As expected, the peak of fluorescence intensity for the labeled boutons doubles as it shifts from 435 units to 850 units (Figure 4D), suggesting one more vesicle has been internalized within the plateau state.

Taken together, we conclude that, after single vesicle fusion, two distinct vesicles are retrieved, one by the end of the initial state, the other by the end of the plateau state. The temporal separation of their internalizations and subsequent acidification lead to the two-phase of acidification observed in SypHluorin experiments. It is generally believed that, in the central synapses, the number of endocytosed vesicles is in tight balance with the number of preceding exocytosed vesicles in order to maintain the stability of the lipid and protein composition in plasma membrane as well as the vesicle pool. Paradoxically, this tight coupling doesn't hold at a single vesicle level, base on our observation. Does it hold at the level of multiple vesicle fusions? To answer this question, we decided to examine the correlation between exocytosis and endocytosis upon multiple vesicle release. We used SypHluorin to measure the number of exocytosed vesicles triggered by a given stimulation in individual synapses. In a parallel experiment, the number of endocytosed vesicles in response to the same stimulation was estimated by FM 1-43 uptake. To trigger different number of released vesicles, we stimulated boutons with 2, 5, 10, 20, and 30 action potentials at 20Hz respectively. Figure 4E shows the plot of endocytosed vesicle number as a function of exocytosed vesicle number. Under stimulation of 2AP and 5AP, the number of endocytosed vesicles per synapse was twice that of exocytosed vesicles (0.65 ± 0.02 vesicles for 2AP, and 1.25 ± 0.03 vesicles for 5AP), consistent with our previous observation upon single vesicle release. However, as the number of exocytosed vesicles increased with more AP stimulations (3.1 ± 0.06 vesicles for 10AP, 4.7 ± 0.09 vesicles for 20AP, and 5.4 ± 0.13 vesicles for 30AP), almost exactly the same number of vesicles were endcocytosed. Therefore, the very tight coupling between exocytosis and endocytosis is re-established when multiple vesicles are released.

Newly Exocytosed SypHluorins Were Preferentially Retrieved in Both Endocytosis

Two endocytosis models have been proposed for small synapses. In the "classical clathrin-mediated endocytosis" model, the vesicle fully collapses onto the plasma membrane and its proteins mix with surface proteins before the subsequent endocytosis (Heuser and Reese, 1973). In the "kiss-run" model, the vesicle connects with the plasma membrane very briefly through a transient fusion pore without losing its protein identity (Ceccarelli et al., 1973). To

test these two models, we examined the protein composition in the newly retrieved vesicles by selectively silencing the fluorescence of surface proteins through photobleaching, as previously described (Fernandez-Alfonso et al., 2006; Wienisch and Klingauf, 2006). We first estimated the relative number of SypHluorin molecules present on the surface by applying a transient extracellular acidification before evoking single vesicle fusion (Figure 5A). Coincidentally, we found that the amount of SypHluorins on the bouton surface at rest is almost equal to that inside a single vesicle. We then photobleached neurons for about 8 minutes that effectively reduced the surface fluorescence to less than 7% of original, without affecting the functions of endocytosis machinery (Supplementary Figure 7). After that, single action potential was applied to evoke single vesicle fusion event. Similar to the responses from control boutons without photobleaching, the fluorescence intensity change also exhibited two-step decay after photobleaching (Figure 5B). However, the changes in both steps were decreased. Thus, a certain degree of mixing occurred between the newly exocytosed vesicular proteins and the surface proteins prior to vesicle retrieval for both steps. This result in general, is in disagreement with the predication based on “kiss-run” model. Specifically, the fluorescence change in the fast step was reduced from 56% to 46%, revealing a preferential recapture of the newly exocytosed vesicular proteins by the fast endocytosis (Figure 5D, E). We further calculated that the retrieved vesicle consisted of 82.9% vesicular SypHluorins and 17.1% surface SypHluorins. Based on these calculations, the chance for each vesicular SypHluorin being retrieved by the fast endocytosis is four times higher than its surface counterpart. Meanwhile, photobleaching is more effective on diminishing the fluorescence change in the slow step, by reducing it from 52% to 28% (Figure 5D, E). The vesicle retrieved by the slow endocytosis has a protein composition of 54 % vesicular SypHluorins and 46% surface SypHluorins. Taking into account that 54% of vesicular SypHluorins and 90% of surface SypHluorins were remained on the surface after the fast endocytosis, we further conclude that, similar to the fast endocytosis, the slow endocytosis also preferentially recapture vesicular SypHluorins, with the chance for each vesicular SypHluorin being retrieved 1.8 times higher than its surface counterpart. In summary, after a single vesicle fusion, ~ 74% of the newly exocytosed SypHluorins were recycled back to the vesicle pool, along with 25% ~ 33% of SypHluorins from the surface.

Clathrin Knockdown by RNAi Inhibits both the Fast and Slow Endocytosis

To further investigate the molecular mechanisms underlying the two temporally distinct endocytosis, we examined the clathrin-dependence of both endocytosis by using RNAi knockdown of clathrin heavy chain (CHC), as previously described (Granseth et al., 2006). The efficiency of RNAi knockdown was measured by fluorescent transferrin uptake. We found that, three days after transfection, transferrin uptake was reduced to ~50% in CHC-RNAi transfected neurons compared with neurons transfected with scrambled RNAi (Supplementary Figure 8). Consistent with partial depletion of CHC by RNAi, the fluorescence intensity decay after single vesicle fusion exhibited arrays of kinetic shapes that likely reflected different degrees of CHC inhibition (Figure 6A). Within the 40s time-measurement window of recording, 42% of traces failed to display fast endocytosis events (Figure 6B middle). Remaining 58% of traces showed detectable fast endocytosis events with an amplitude of SypHluorins retrieval being slightly decreased compared to the control (Figure 6B middle and right). Meanwhile, slow endocytosis events were obliterated from 76% of traces (Figure 6C middle). For the rest of traces (~24%), slow endocytosis events can be detected and the amplitude of SypHluorins retrieval was not significantly different from control (Figure 6C middle and right). Finally, for 41–42% of the vesicles undergoing fusion, neither fast endocytosis nor slow endocytosis was observed during the entire recording time.

Events whose fluorescence failed to decay within the time-measurement window are presumably caused by stronger inhibitions of CHC, as shown in the third trace of Figure 6A and in previous report (Granseth et al., 2006). While these recordings certainly showed the significant effect of CHC depletion on vesicular protein retrieval, further analysis of these "flat" traces is no longer informative. On the other hand, because RNAi only partially depleted CHC in our experiments, we reasoned that kinetic analysis of intermediate states resulting from partial CHC inhibition could provide more detailed information on whether each of endocytic steps might be differentially affected by clathrin depletion. Indeed, analyses of the dwell time distributions of the fast and slow endocytosis revealed that both endocytosis were significantly delayed by RNAi knockdown, with the fast endocytosis deferred from 2.7 ± 0.1s to 5.8 ± 0.3s and the slow endocytosis from 17.9 ± 0.1s to 26.1 ± 1.6s (Figure 6D and 6E). In contrast, the number of proteins retrieved by the fast or slow endocytosis is not substantially reduced by partial depletion of clathrin (Figure 6B and 6C). These observations suggest that while partial CHC depletion slows down the speed of vesicle retrieval, it does not significantly reduce the amount of proteins retrieved by each vesicle if the retrieval actually takes place. Should this be the case, there might be more events took place after 40s due to the inhibition of CHC, but were not detected during our time-measurement window.

Activity-Dependence of the Fast and Slow Endocytosis

In addition to the activity-dependent vesicle recycling, which is highly regulated and precisely timed, spontaneous synaptic vesicle recycling has also been demonstrated in hippocampal neurons by using FM dye (Groemer and Klingauf, 2007; Murthy and Stevens, 1999; Sara et al., 2005). In agreement with these reports, we also observed that vesicles were retrieved randomly in the absence of action potentials by using SypHluorins (Figure 7A, B) and FM 1-43 (Figure 7F). This kind of spontaneous retrieval occurs with a rate of 36% of the vesicle per synapse in every 40s. Interestingly, for synapses in which action potentials failed to evoke vesicle release, the spontaneous retrievals became synchronized, with a delay time at minimum of 5 seconds (Figure 7C, D). Thus, it is likely that spontaneous endocytosis can be converted to a more regulated form in the presence of action potentials.

For the following reasons, we believe the fast endocytosis (~3 seconds) is directly linked to the action potential-triggered exocytosis. First, it is tightly time-locked to the rapid exocytosis (Figure 2D, δ = 1.1s). Second, for synapses in which action potentials failed to trigger exocytosis, the endocytosis occurs with a delay longer than 5 seconds, usually around 15 seconds, significantly slower than the fast endocytosis. Third, when the boutons were bathed in 10μM FM 1-43 for 6s (time required to complete the fast endocytosis) in the absence of action potentials, no dye-labeled vesicles could be detected (Figure 7E). This observation suggests the fast endocytosis observed after the stimulation (Figure 4C) was indeed trigged by the action potential.

On the other hand, the slow endocytosis that occurs after a 10 second delay is likely a form of "regulated spontaneous endocytosis". The temporal distribution of the "slow endocytosis" was much broader (Figure 2E, δ = 5s when fitted with Gaussian), and resembled that of the "regulated spontaneous endocytosis" (Figure 7D). We took this as one clue that an action potential may convert spontaneous endocytosis to the slow endocytosis. However, there are important differences between these two forms of endocytosis. Although the slow endocytosis occurs exclusively when a stimuli succeeds to evoke vesicle fusions, the "regulated spontaneous endocytosis" occurs at estimated rate of 44% in failures. It is possible that the exocytosed proteins function as signals to enhance the rate of "regulated spontaneous endocytosis". However, we cannot exclude the possibility that the slow endocytosis and the "regulated spontaneous endocytosis" might each involves very different mechanisms.

Activity Affects the Usage of Two Endocytosis Pathways

After characterizing the properties of the fast and slow endocytosis at the level of single vesicle fusion, we extended our investigation to multiple vesicle fusion events. We asked whether one pathway might become more predominant when more vesicles were released by stronger stimulation, or in another word, can neuron activity affect the usage of two endocytosis pathways by synapses?

Because the fast endocytosis may initiate as early as 0.8s after stimulation, we restricted the stimulation duration within 0.5 s period to eliminate the endocytosis events during the exocytosis. We stimulated neurons at the frequencies of 1Hz, 5Hz, 10Hz, 20Hz and 30Hz. Such stimulations normally trigger 1 to 5 vesicle releases. The time courses of fluorescence intensity change after various vesicle fusions are shown in Figure 8A. We observed that the majorities of fusion events (85%, 95%, 75%, 80%, and 78% for 1, 2, 3, 4 and 5 vesicles, respectively) were followed by “two-phase” fluorescence decay. Thus, the fast and slow endocytosis operated in parallel under these conditions.

We further examined whether increasing the number of exocytosed vesicles resulted in a preferential usage of one endocytosis pathway over the other. Fitting the fluorescence intensity change by two-phase of endocytosis model allowed us to compare the dwell time distributions (Figure 8B), fractional retrieval of SypHluorins (Figure 8C), dwell times (Figure 8D) and decay time constants (Figure 8E) after various vesicle fusions for both the fast and slow endocytosis. When the number of exocytosed vesicles was increased from one to five, a larger fraction of SypHluorins was retrieved by the slow endocytosis (54% ± 2% for one vesicle and 69% ± 2% for five vesicles), whereas the fractional retrieval by the fast endocytosis was decreased (55% ± 2% for one vesicle and 38% ± 2% for five vesicles) (Figure 8C). Meanwhile, the dwell time of the slow endocytosis was advanced from 18.7 ± 0.5 seconds for one vesicle to 13.0 ± 0.6 seconds for five vesicles (Figure 8B, Figure 8D). In comparison, the dwell time for the fast endocytosis remained unchanged up to five vesicle fusions (Figure 8B, Figure 8D). The decay time constant for the slow endocytosis increased from 3.0 ± 0.3 seconds to 10.3 ± 0.5 seconds, whereas the decay time constant for the fast endocytosis was unaffected by the number of exocytosed vesicles (Figure 8E). Note that with one vesicle being endocytosed, the decay time constant was dictated solely by reacidification. However, when multiple vesicles were retrieved, time constant was dependent to a larger extent on the range of retrieval times for varies vesicles as well as reacidification. In summary, these results suggest that the fast endocytosis is less susceptible to the increased number of exocytosed vesicles than the slow endocytosis, which in contrast, becomes the more predominant mechanism for recapturing the exocytosed proteins under stronger stimulation. Interestingly, a shift of protein retrieval to the slow pathway (Figure 8C) was not at the cost of overall slowing down of retrieval rate. Although a larger fraction of vesicle retrieval was mediated by the “slow pathway” with more vesicles being exocytosed, the dwell time for the “slow pathway” was also shortened under the same condition (Figure 8D). Consequently, normalized average responses showed similar speeds of recapturing SypHluorin reporters over a certain range of released vesicles (Figure 8F). Thus, although the preferential usage of the two endocytosis pathways was affected by the stimulation intensity, endocytosis was able to maintain a relatively steady rate within a certain range, in agreement with previous reports (Balaji et al., 2008; Granseth et al., 2006).

What are the mechanisms underlying the activity-dependent usage of different endocytosis pathways? One immediate insight is that the Ca^{2+} elevation in presynaptic terminals during stimulation might regulate the fast and slow endocytosis in a different way. To test this possibility, we examined the Ca^{2+}- dependence of each endocytosis at the level of single vesicle fusion. In order to attain single vesicle fusion events at different presynaptic Ca^{2+} concentration ($[Ca^{2+}]_{in}$), we stimulated neurons with 3 action potentials at 20Hz while

changing external Ca^{2+} concentration ($[Ca^{2+}]_{ex}$) from 1mM to 5mM. The action potential-triggered presynaptic Ca^{2+} transients in different $[Ca^{2+}]_{ex}$ were measured by the low affinity Ca^{2+} indicator Magnesium Green AM (K_d ~ 6μM), and a near-linear relationship was observed between the peak change in $[Ca^{2+}]_{in}$ and $[Ca2+]_{ex}$ (Supplementary Figure 9). We next examined the endocytic events subsequent to single vesicle fusion in different $[Ca^{2+}]_{ex}$ (Figure 8G). In Figure 8 H- J, we present the effects of $[Ca^{2+}]_{ex}$ on the fractional retrieval, dwell time and decay time constant for both the fast and slow endocytosis. In agreement with the activity-dependent regulation of the slow endocytosis observed from multiple vesicle fusions (Figure 8D), increasing $[Ca^{2+}]_{ex}$ (and by extension $[Ca^{2+}]_{in}$) significantly accelerated the slow endocytosis after single vesicle fusion, with the dwell time advanced from 18.2 ± 0.5 seconds for 1mM to 14.7 ± 0.5 seconds for 5mM (Figure 8I). In contrast, the dwell time for the fast endocytosis was largely unaffected by $[Ca^{2+}]_{ex}$. Meanwhile, increasing $[Ca2+]_{ex}$ had no significant effects on the fractional retrieval of SypHluorins (Figure 8H) and decay time constant (Figure 8J) for both the fast and slow endocytosis. Together, these observations indicate that Ca^{2+}, as an important modulator for endocytosis, specifically controls the speed of slow endocytosis without affecting the fast endocytosis. Furthermore, the different regulatory roles of Ca^{2+} in the fast and slow endocytosis imply that down-stream molecular events modulated by Ca^{2+} signaling might be responsible for dividing the different endocytic pathways.

Two-phase of Endocytosis Detected by vGlut1-pHluorin

A newly developed fluorescent sensor vGlut1-pHluorin, with pHluorin fused to the first intravesicular loop of vGlut1, showed great improvement on the signal to background ratio over the original synaptopHluorin (Voglmaier et al., 2006). It has been used successfully to study vGlut1 endocytosis and single vesicle recycling (Balaji and Ryan, 2007). Next, we examined whether the endocytosis of vGlut1-pHluorin after single vesicle fusion also proceed in two phases, as previously observed in SypHluorin.

First, we calibrated the quantal vGlut1-pHluorin fluorescence intensity of single vesicle exocytosis (Fig. 9A). Based on 533 fluorescence responses to single stimuli from 65 synapses, we estimated the standard deviation of baseline noise as 37.9 fluorescence units and the mean single vesicle fluorescence as 181.4 units with a standard deviation of 51.4 units. Therefore, in our detecting system, the signal to noise ratio for detecting single vesicle fusion events with vGlut1-pHluorin was about 4.8, very similar to that of SypHluorin.

We next characterized the time course of fluorescence intensity change after single vesicle exocytosis (Δ*F* within the mean single vesicle fluorescence ± standard deviation). We found that 80.5% (95 out of 118 traces) of single vesicle recordings exhibited “two-phase” of fluorescence decay, similar to the pattern observed from SypHluorin reporters. Kinetic analyses further revealed that the fast fluorescence decay was initiated at 2.5 ± 0.2 s after exocytosis (Figure 9D), with a decay amplitude about half of the quantal size (0.51 ± 0.01) and a decay time constant (τ1) of about 1.5 ± 0.2s (Figure 9G). The slow fluorescence decay was initiated at 14.4 ± 0.4 s (Figure 9E), with a decay amplitude also about half of the quantal size (0.54 ± 0.02) and a decay time constant (τ2) of 2.2 ± 0.2s (Figure 9H). The combined dwell time distribution suggests the fast and slow endocytosis belong to two temporally distinct populations (Figure 9F). Thus, vGlut1 was also retrieved by the fast and slow endocytosis pathways in parallel, as was Synaptophysin.

Discussion

Our essential observation is that single vesicle fusion is followed by two distinct vesicles recoveries, with its protein components systematically distributed into two distinct daughter vesicles. Similar observation was also obtained from SypHluorin 1x and SypHluorin 2x

(Supplementary Figure 3). Two recent papers using other forms of pHluorin reporters reached a quite different conclusion from ours (Balaji and Ryan, 2007; Granseth et al., 2006), but methodological differences may account for most of the differences. Balaji et al employed vGlut1-pHluorin to track exocytosis and endocytosis of individual vesicles at the single-molecule level (Balaji and Ryan, 2007). By analyzing the kinetic steps from exocytosis to reacidification of the retrieved vesicle, these researchers conclude that each synaptic vesicle fusion is followed by a single stochastic mode with an average time of 14s, and the fast endocytosis is just one end of the distribution of times of this common process. In our study, the multiple copies of SypHluorin 4x and vGlut1-pHluorin in each vesicle provide evidence for two distinct retrieval events, instead of one expected from the single-molecule trafficking. The combined distribution of dwell times from fusion pore opening to both retrieval events (Figure 2F and Figure 9F) strongly suggest that these two events are kinetically distinct. In another work, Granseth et al. used a synaptophysin-based pHluorin reporter very similar to ours for monitoring the single vesicle exocytosis and endocytosis (Granseth et al., 2006). Because the reporter did not have a signal-to-noise ratio adequate to resolve individual vesicles, these authors averaged fluorescence responses over a population of synapses and found a simple exponential decay of fluorescence following stimulation. Based on their analysis, they reached the conclusion that only a slow mode of endocytosis with a time constants of 15s operates at hippocampal synapses. When we average our individual vesicle responses, we also see what could be described as a single exponential with a time constant of about 20 seconds (Supplementary Figure 1). However, as we have shown above, when individual vesicles are tracked, the decay of fluorescence actually reflects a combination of two distinct vesicles recovery.

The kinetics of the fast vesicle recovery that we observed is similar to the fast mode (kiss-and-run) described by Gandhi and Stevens (Gandhi and Stevens, 2003). However, our present observations differed from those of Gandhi and Stevens in three other ways. First, the time from fusion pore opening to the internalization (~3 seconds) was significantly longer than 400–860ms. Second, the acidification time constant we observed (3 seconds) was about 4 times longer that the 850 ms reported earlier. Third and most importantly, we found half of the fluorescence remained by the end of the fast endocytosis instead of the fully recovery in the previous work.

The fundamental distinctions between ‘kiss-and-run’ vs. ‘classical clathrin-mediated pathway’ of vesicle cycling are related to two properties: the time course for internalization (Aravanis et al., 2003; Gandhi and Stevens, 2003; Richards et al., 2005) and whether or not the vesicle identity was maintained after use (Ceccarelli et al., 1973; Fernandez-Alfonso et al., 2006; Wienisch and Klingauf, 2006). Although the fast endocytosis in our observation provides a relative fast speed of vesicle retrieval, it differs from the conventional ‘kiss-and-run’ in an essential way: the vesicle identity is only partially preserved. The slow endocytosis resembles the ‘classical clathrin-mediated pathway’ in both time course (10 ~20s) and the nature of partial retrieval of newly released proteins.

Our results from CHC RNAi knockdown experiment are, to a large extent, in agreement with previous report by Granseth et al (Granseth et al., 2006). Even though we were not able to achieve a complete inhibition of CHC, we found that about 42% of traces obtained from RNAi knockdown neurons failed to display any sort of decay during experiment time window. These observations suggest that that both fast and slow endocytosis were sensitive to CHC knockdown, although the effects of knockdown on vesicle endocytosis can be indirect, as discussed below. Analyzing the traces of partial block further revealed that knocking down CHC delayed both fast and slow endocytosis without substantially changing the amount of proteins being retrieved by each vesicle. Together with these results, we are inclined to suggest that clathrin might be involved in both fast and slow endocytosis.

Despite that CHC RNAi under our experimental conditions had a significant effect on the rate of endocytosis, and in some extreme cases, endocytosis was completed abolished, we can not merely draw a conclusion that clathrin is directly involved in the fast and slow endocytosis described in this research. There were some main drawbacks of the CHC RNAi knockdown approach. For example, clathrin plays critical roles in a lot of cellular process other than synaptic vesicle recycling. A chronic reduction in clathrin-mediated process such as protein trafficking, sorting and transportation may also alter synaptic vesicle endocytosis indirectly. For these reasons, caution must be exercised when interpreting the results of chronic CHC reduction. Improved methodologies, such as acute clathrin inactivation, may be employed in future experiments to further elucidate the roles of clathrin in synaptic vesicle endocytosis at central synapses.

In order for neurons to maintain high rate of action potential firing (normally greater than 10Hz), the recapture and reformation of synaptic vesicles must be carried out in a highly efficient way. Meanwhile, the precise control of the membrane composition of presynaptic terminals is critical for the synaptic transmission, morphology, growth, and other signaling events. The two pathways of endocytosis we observed may be dedicated to accomplish these tasks coordinately. The fast endocytosis serves to transport the exocytosed vesicular proteins back to the vesicle pool rapidly, whereas, the slow endocytosis is set to clean up the residual left behind. As a result, the protein compositions of the synaptic vesicle pool and plasma membrane pool are efficiently reconstituted within a short time (~30s).

Our interpretation has been based on the assumption that a presynaptic terminal releases only one synaptic vesicle per action potential. However, we cannot fully exclude the possibility that a single action potential consistently triggers fusion of two vesicles at the same time. Such coordinated multivesicular fusion has been recently demonstrated at ribbon synapses (Singer et al., 2004). However, if the quantal SypHluorin fluorescence response estimated in our study (Figure 1F) indeed represented two vesicle fusion events instead of one, the exocytosis-endocytosis coupling presented in Figure 4E will be converted to a new form of relationship plotted in Supplementary Figure 6. By this scenario, the new exocytosis-endocytosis relationship would suggest that the tight coupling holds at single action potential level, but will be disrupted when more vesicles are released by high frequency stimulation. In the end, the exocytosed vesicles may outnumber the endocytosed vesicles by nearly two-fold. Such outcome will make it very difficult for a synapse to maintain the membrane compositions of the synaptic vesicle pool and plasma membrane pool during the normally high frequency of firing. Thus, we favor the assumption that a single action potential triggers one vesicle fusion in this study. If later works were to reveal that a single action potential consistently triggers fusion of two vesicles at hippocampal synapses and other mechanisms may compensate the exocytosis-endocytosis uncoupling at high frequency of stimulation, our observations should be reinterpreted accordingly.

It has been demonstrated that elevation of intracellular Ca^{2+} concentration accelerates the endocytosis rate in several synapses (Neves et al., 2001; Sankaranarayanan and Ryan, 2001; Wu et al., 2005). Here, we found that increasing stimulation frequency or elevating presynaptic Ca^{2+} concentration specifically accelerated the slow endocytosis, without affecting the fast endocytosis. Therefore, Ca^{2+} might serve as the initiator for an activity-dependent switch between different mechanisms of synaptic vesicle recycling. Although detailed molecular mechanisms are not yet understood, it is likely that Ca^{2+} influx can trigger a cascade of molecular events that ultimately affects the slow endocytic pathway. Dephosphins are a group of endocytic proteins that can be dephosphorylated by Ca^{2+}-dependent phosphatase calcineurin during depolarization (Cousin and Robinson, 2001). After the termination of action potentials, the dephosphins can be rephosphorylated by protein kinases such as Cyclin-dependent kinase 5 (Cdk5), which rephosphorylates at least

three dephosphins: dynamin 1, PIPKIγ, and synaptojanin. It has been reported the calcineurin/cdk5-dependent phosphorylation cycle of the dephosphins is essential for synaptic vesicle endocytosis (Tan et al., 2003). Interestingly, a recent study revealed that this phosphorylation cycle specifically regulates a slow form of endocytosis, without affecting the fast form of endocytosis (Evans and Cousin, 2007). Although the definitions for the fast and slow endocytosis in Evans & Cousin (2007) might not be exactly the same as those presented in our study, the role of Ca^{2+} in selective regulation of endocytic pathways is very similar to our observation. Therefore, future studies directed towards calcineurin/cdk5-dependent phosphorylation cycle of the dephosphins may provide important insight into how the fast and slow endocytosis is controlled. In addition to the dephosphins, other endocytic proteins have also been reported to mediate different pathways, such as clathrin adaptors AP2 and AP3 (Voglmaier et al., 2006) and different family members of dynamin (Ferguson et al., 2007). It would be of great interest to examine the involvement of these key mediators in the fast and slow endocytosis reported here. Resolving the divergent mechanisms underlying different endocytosis pathways is not only essential for understanding the architecture and function of the highly efficient endocytosis machinery, but also crucial for uncovering the regulatory mechanisms underlying the coordinated contributions of different endocytic pathways, in response to the constantly changing network.

Experimental Procedures

DNA constructions

To permit insertion of pHluorin into the luminal domain between transmembrane domain 3 and 4 of synaptophysin, we first created a unique EcoR V site at position 184–185 of rat synaptophysin sequence (NP_036796). The resulting plasmid was digested by EcoR V to generate a vector backbone for blunt end ligation. To facilitate cloning, DNA sequence coding for ‘super-ecliptic pHluorin’ was first cloned into the TOPO cloning vector (Invitrogen, Carlsbad, CA). Up to four pHluorin units with the same reading frame were eventually inserted into TOPO vector in a step-by-step manner. Ligation inserts were further generated by releasing one or more pHluorin units from the TOPO vectors and were subsequently inserted into the ligation backbone described before. Detailed sequence information can be obtained by contacting the authors.

Cell culture and transfection

Hippocampal CA1-CA3 neurons from postnatal day 0 (P0) rats were cultured as previously described (Murthy et al., 1997). After 6–7 days in culture, cells were transfected by using the calcium phosphate gene transfer method (Xia et al., 1996). Transfected cultures were allowed to grow for at least another week. For Clathrin RNAi or clathrin-AP180 expression experiments, neurons were transfected 3 days before recording, as described previously(Granseth et al., 2006). Imaging was performed at room temperature when cells were 14–19 days old in vitro.

Stimulation and Imaging

For imaging experiments, coverslips were mounted in a stimulation chamber on a movable stage. Field stimulation used a pair of platinum bath electrodes that delivered pulses producing a 10 V/cm gradient across the chamber. All experiments, except as otherwise noted, were done in the extracellular media containing (in mM), 136 NaCl, 2.5 KCl, 10 glucose, 10 HEPES, 2 $CaCl_2$, and 1.3 $MgCl_2$ at room temperature, with final pH of 7.3. 10μM NBQX, and 50 μM DL-APV were added to block recurrent activity. Acidic extracellular solution with final pH of 5.6 was prepared by replacing HEPES in the standard media with MES (pK_a = 6.1). Bafilomycin A1 (Calbiochem) was used at 1 μM (0.2%

DMSO) and applied for 60 s before stimulation. All chemicals were obtained from Sigma, unless otherwise noted.

To label synaptic vesicles with FM 1-43, the cells were perfused with extracellular media containing 10 μM FM 1-43 (Molecular Probes, Eugene, OR) by using a bulk perfusion system (VC-6 Perfusion Valve Control System, Warner Instruments, Hamden, CT). Following a 7 s delay (to allow for dye equilibration with membranes, Supplementary Figure 5A), variable numbers of action potentials was applied. After designated dye exposure time, dye-free washing solution (with 0.5mM Ca^{2+}, 10mM Mg^{2+}) containing 1 mM ADVASEP 7 (CyDex, Inc) was perfused for 1 minute by using a fast local perfusion system (VC-6M Mini-Valve System combined with SF-77B perfusion stepper system, Warner Instruments, Hamden, CT). This was followed by another 7 minutes of washing with dye free solution without ADVASEP 7 through bulk bath perfusion. After the wash, we acquired an image of the stained synapses and then took another image after destaining (1200 APs at 10 Hz). The rapid local control of FM 1-43 perfusion and ADVASEP 7 washing allowed ~90% of FM1-43 to be washed out within 0.7 s after designated dye exposure time (Supplementary Figure 5B). 1 μM TTX was added to dye-containing medium during FM 1-43 labeling of spontaneous endocytosis. Extracellular acidification experiment was also carried out by using the local rapid perfusion system.

Imaging and Quantification

Images were acquired at 30 Hz with a Hamamatsu EB CCD C7190 intensified camera (Hamamatsu Corporation, Japan) connected to an Olympus inverted microscope (IX70) through a 40X, 1.30 NA oil objective. Both SypHluorins and FM 1-43 fluorescence were excited by 460–500nm light from a mercury lamp, and collected through a 510nm long-pass filter.

Images were analyzed with SimplePCI (Compix Inc., Cranberry Township, PA). The active boutons were identified by subtracting the 60-frame average before the stimulation from the 60-frame average right after the 20 AP stimulation at 20Hz. The total fluorescence intensity was obtained from circular Regions of interest (ROI) of 1.6μm diameters around isolated bright spots. The baseline fluorescence was obtained by averaging 150 images (~5s) at rest previous to the stimulus. Before most of the analysis, SypHluorin fluorescence responses were corrected for their baseline fluorescence and photobleaching.

Supplementary Material

Refer to Web version on PubMed Central for supplementary material.

Acknowledgments

We thank Dr. Charles F. Stevens for providing laboratory space and experimental instruments to carry out this study, and his insightful advice throughout the work. We thank Dr. Wolfhard Almers for critical reading of the manuscript and insightful comments. The work was supported in part by the Howard Hughes Medical Institute and in part by NIH (S.F.H).

References

Aravanis AM, Pyle JL, Tsien RW. Single synaptic vesicles fusing transiently and successively without loss of identity. Nature 2003;423:643–647. [PubMed: 12789339]

Balaji J, Armbruster M, Ryan TA. Calcium control of endocytic capacity at a CNS synapse. J Neurosci 2008;28:6742–6749. [PubMed: 18579748]

Balaji J, Ryan TA. Single-vesicle imaging reveals that synaptic vesicle exocytosis and endocytosis are coupled by a single stochastic mode. Proc Natl Acad Sci U S A 2007;104:20576–20581. [PubMed: 18077369]

Ceccarelli B, Hurlbut WP, Mauro A. Turnover of transmitter and synaptic vesicles at the frog neuromuscular junction. J Cell Biol 1973;57:499–524. [PubMed: 4348791]

Cousin MA, Robinson PJ. The dephosphins: dephosphorylation by calcineurin triggers synaptic vesicle endocytosis. Trends Neurosci 2001;24:659–665. [PubMed: 11672811]

Evans GJ, Cousin MA. Activity-dependent control of slow synaptic vesicle endocytosis by cyclin-dependent kinase 5. J Neurosci 2007;27:401–411. [PubMed: 17215401]

Ferguson SM, Brasnjo G, Hayashi M, Wolfel M, Collesi C, Giovedi S, Raimondi A, Gong LW, Ariel P, Paradise S, et al. A selective activity-dependent requirement for dynamin 1 in synaptic vesicle endocytosis. Science 2007;316:570–574. [PubMed: 17463283]

Fernandez-Alfonso T, Kwan R, Ryan TA. Synaptic vesicles interchange their membrane proteins with a large surface reservoir during recycling. Neuron 2006;51:179–186. [PubMed: 16846853]

Fesce R, Grohovaz F, Valtorta F, Meldolesi J. Neurotransmitter release: fusion or 'kiss-and-run'? Trends Cell Biol 1994;4:1–4. [PubMed: 14731821]

Gandhi SP, Stevens CF. Three modes of synaptic vesicular recycling revealed by single-vesicle imaging. Nature 2003;423:607–613. [PubMed: 12789331]

Granseth B, Odermatt B, Royle SJ, Lagnado L. Clathrin-mediated endocytosis is the dominant mechanism of vesicle retrieval at hippocampal synapses. Neuron 2006;51:773–786. [PubMed: 16982422]

Groemer TW, Klingauf J. Synaptic vesicles recycling spontaneously and during activity belong to the same vesicle pool. Nat Neurosci 2007;10:145–147. [PubMed: 17220885]

Heuser JE, Reese TS. Evidence for recycling of synaptic vesicle membrane during transmitter release at the frog neuromuscular junction. J Cell Biol 1973;57:315–344. [PubMed: 4348786]

Klingauf J, Kavalali ET, Tsien RW. Kinetics and regulation of fast endocytosis at hippocampal synapses. Nature 1998;394:581–585. [PubMed: 9707119]

Li Z, Burrone J, Tyler WJ, Hartman KN, Albeanu DF, Murthy VN. Synaptic vesicle recycling studied in transgenic mice expressing synaptopHluorin. Proc Natl Acad Sci U S A 2005;102:6131–6136. [PubMed: 15837917]

McMahon HT, Bolshakov VY, Janz R, Hammer RE, Siegelbaum SA, Sudhof TC. Synaptophysin, a major synaptic vesicle protein, is not essential for neurotransmitter release. Proc Natl Acad Sci U S A 1996;93:4760–4764. [PubMed: 8643476]

Miesenbock G, De Angelis DA, Rothman JE. Visualizing secretion and synaptic transmission with pH-sensitive green fluorescent proteins. Nature 1998;394:192–195. [PubMed: 9671304]

Murthy VN, Sejnowski TJ, Stevens CF. Heterogeneous release properties of visualized individual hippocampal synapses. Neuron 1997;18:599–612. [PubMed: 9136769]

Murthy VN, Stevens CF. Synaptic vesicles retain their identity through the endocytic cycle. Nature 1998;392:497–501. [PubMed: 9548254]

Murthy VN, Stevens CF. Reversal of synaptic vesicle docking at central synapses. Nat Neurosci 1999;2:503–507. [PubMed: 10448213]

Neves G, Neef A, Lagnado L. The actions of barium and strontium on exocytosis and endocytosis in the synaptic terminal of goldfish bipolar cells. J Physiol 2001;535:809–824. [PubMed: 11559777]

Pyle JL, Kavalali ET, Piedras-Renteria ES, Tsien RW. Rapid reuse of readily releasable pool vesicles at hippocampal synapses. Neuron 2000;28:221–231. [PubMed: 11086996]

Richards DA, Bai J, Chapman ER. Two modes of exocytosis at hippocampal synapses revealed by rate of FM1-43 efflux from individual vesicles. J Cell Biol 2005;168:929–939. [PubMed: 15767463]

Richards DA, Guatimosim C, Betz WJ. Two endocytic recycling routes selectively fill two vesicle pools in frog motor nerve terminals. Neuron 2000a;27:551–559. [PubMed: 11055437]

Richards DA, Guatimosim C, Betz WJ. Two endocytic recycling routes selectively fill two vesicle pools in frog motor nerve terminals. Neuron 2000b;27:551–559. [In Process Citation]. [PubMed: 11055437]

Sankaranarayanan S, Ryan TA. Calcium accelerates endocytosis of vSNAREs at hippocampal synapses. Nat Neurosci 2001;4:129–136. [PubMed: 11175872]

Sara Y, Virmani T, Deak F, Liu X, Kavalali ET. An isolated pool of vesicles recycles at rest and drives spontaneous neurotransmission. Neuron 2005;45:563–573. [PubMed: 15721242]

Singer JH, Lassova L, Vardi N, Diamond JS. Coordinated multivesicular release at a mammalian ribbon synapse. Nat Neurosci 2004;7:826–833. [PubMed: 15235608]

Sudhof TC, Lottspeich F, Greengard P, Mehl E, Jahn R. A synaptic vesicle protein with a novel cytoplasmic domain and four transmembrane regions. Science 1987;238:1142–1144. [PubMed: 3120313]

Takamori S, Holt M, Stenius K, Lemke EA, Gronborg M, Riedel D, Urlaub H, Schenck S, Brugger B, Ringler P, et al. Molecular Anatomy of a Trafficking Organelle. Cell 2006;127:831–846. [PubMed: 17110340]

Takei K, Mundigl O, Daniell L, De Camilli P. The synaptic vesicle cycle: a single vesicle budding step involving clathrin and dynamin. J Cell Biol 1996;133:1237–1250. [PubMed: 8682861]

Tan TC, Valova VA, Malladi CS, Graham ME, Berven LA, Jupp OJ, Hansra G, McClure SJ, Sarcevic B, Boadle RA, et al. Cdk5 is essential for synaptic vesicle endocytosis. Nat Cell Biol 2003;5:701–710. [PubMed: 12855954]

Voglmaier SM, Kam K, Yang H, Fortin DL, Hua Z, Nicoll RA, Edwards RH. Distinct endocytic pathways control the rate and extent of synaptic vesicle protein recycling. Neuron 2006;51:71–84. [PubMed: 16815333]

Wienisch M, Klingauf J. Vesicular proteins exocytosed and subsequently retrieved by compensatory endocytosis are nonidentical. Nat Neurosci 2006;9:1019–1027. [PubMed: 16845386]

Willig KI, Rizzoli SO, Westphal V, Jahn R, Hell SW. STED microscopy reveals that synaptotagmin remains clustered after synaptic vesicle exocytosis. Nature 2006;440:935–939. [PubMed: 16612384]

Wu W, Xu J, Wu XS, Wu LG. Activity-dependent acceleration of endocytosis at a central synapse. J Neurosci 2005;25:11676–11683. [PubMed: 16354926]

Xia Z, Dudek H, Miranti CK, Greenberg ME. Calcium influx via the NMDA receptor induces immediate early gene transcription by a MAP kinase/ERK-dependent mechanism. J Neurosci 1996;16:5425–5436. [PubMed: 8757255]

Zenisek D, Steyer J, Feldman M, Almers W. A membrane marker leaves synaptic vesicles in milliseconds after exocytosis in retinal bipolar cells. Neuron 2002;35:1085. [PubMed: 12354398]

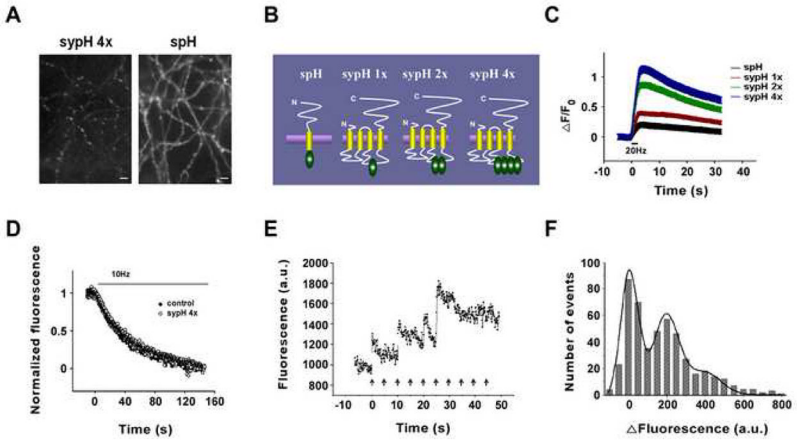

Figure 1. Detection of Single Vesicle Release by SypHluorins

(A) Images of neurons expressing SypHluorin 4x (sypH 4x) or SynaptopHluorin (spH).

(B) Schematic representations of SynaptopHluorin and SypHluorins with 1,2, and 4 phluorin reporters.

(C) Fluorescence response as a function of time for the constructs during stimulation of 40 action potentials at 20Hz. The change in fluorescence intensity (ΔF) was normalized to the fluorescence intensity before stimulation (F0).

(D) Loss of FM4-64 from preloaded control synapses and synapses expressing SypHluorin 4x as a function of time during 10 Hz stimulation.

(E) Bouton fluorescence (arbitrary units) as a function of time during 0.2 Hz stimulation.

(F) Histogram of bouton fluorescence (arbitrary units) for 505 single stimulus presentations. Smooth curve is one expected for quantal releases (see text, $P = 0.99$, χ^2 test, d.f. = 15). Error bars represent SEM

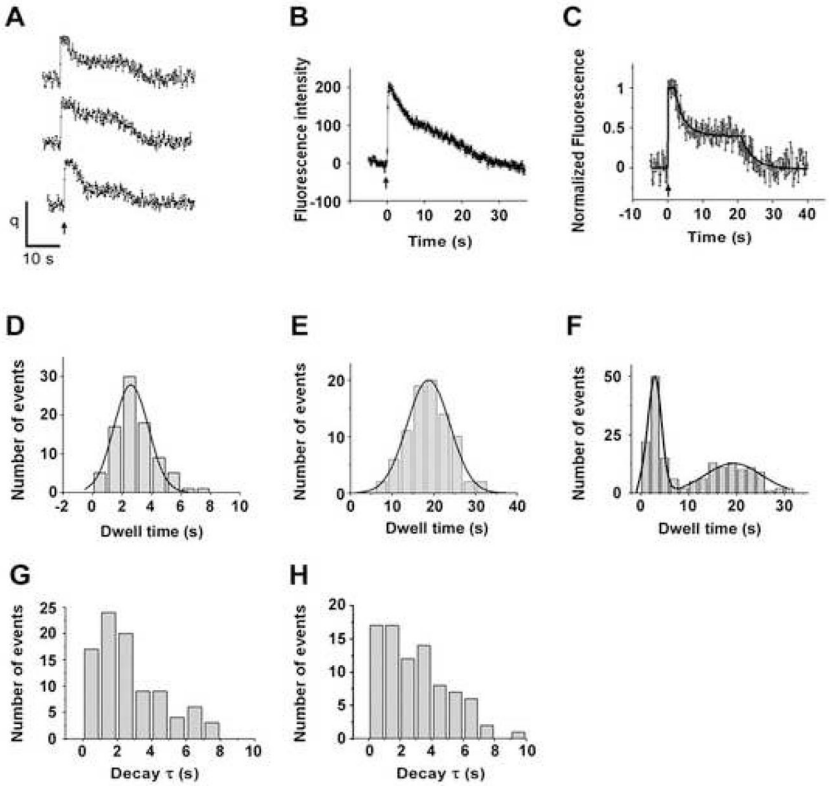

Figure 2. Time Course of Single Vesicle Internalization

(A) Example traces of fluorescence intensity (arbitrary units) as a function of times (s) for single vesicles. Action Potential was delivered at 0s, as indicated by the arrow.

(B) Average of 86 single vesicle responses.

(C) An example fit (black line) of a trace with two distinct phases of exponential decay.

(D) Histogram of dwell time (s) of the initial state (see text) for 86 vesicles. Smooth curve is the fit with Gaussian distribution, yielding a mean of 2.6s with a standard deviation of 1.2s

(E) Dwell time histogram from fusion pore opening to the end of the plateau state. Gaussian fit (shown as smooth curve) yield a mean of 18.2s with a standard deviation of 5.2s.

(F) Distribution of times from fusion pore opening to the end of both states by combining D and E. Smooth curve is the fit with two-component Gaussian distribution, yielding a mean of 2.9s with a standard deviation of 1.4s for the first component, and a mean of 19.3s with a standard deviation of 6.8s for the second component.

(G) Histogram of time constant of the first phase of decay, the mean value is 2.6 ± 0.2s.

(H) Histogram of time constant of the second phase of decay, the mean value is 3.2 ± 0.3s.

Data in (G) and (H) are presented as mean ± SEM

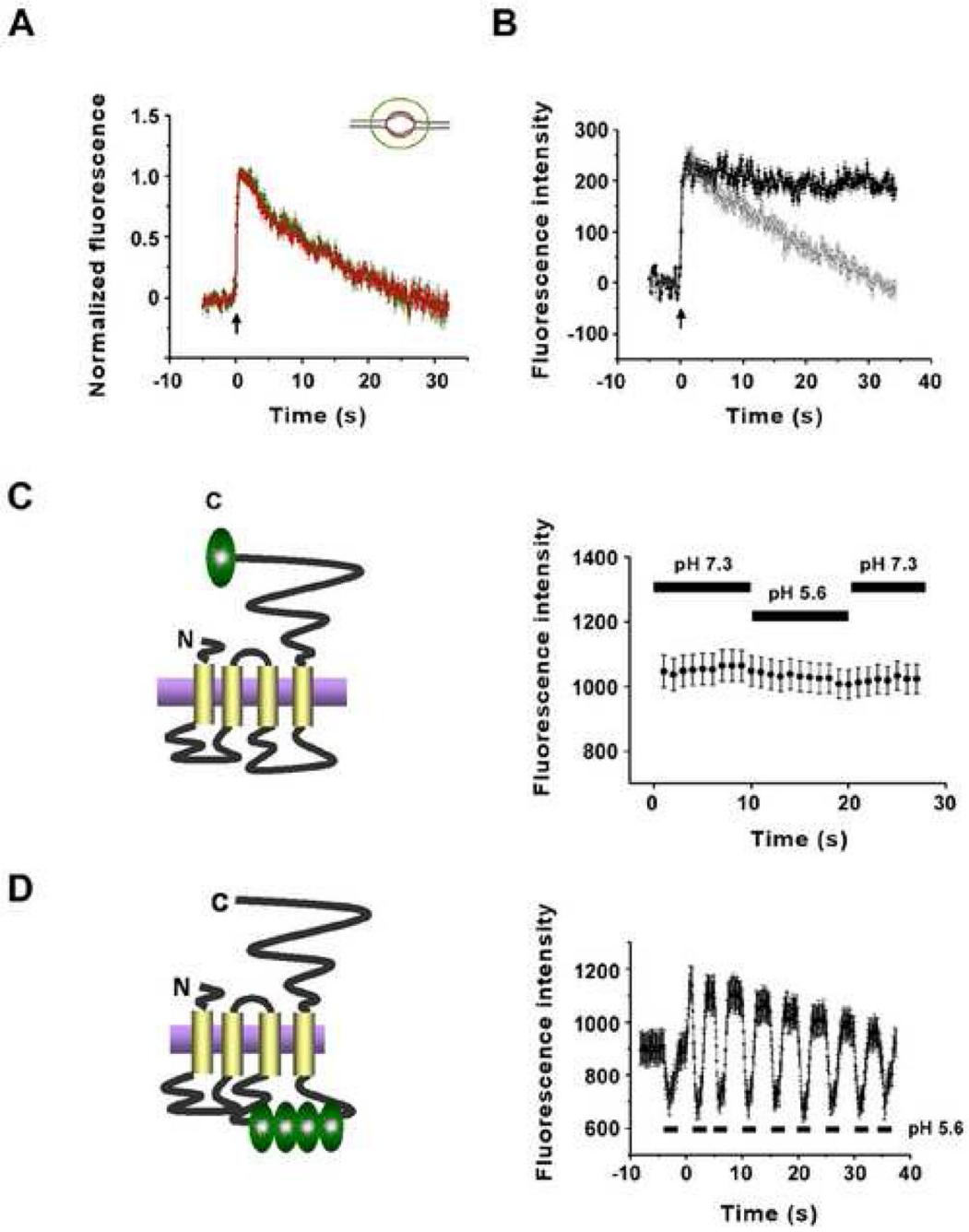

Figure 3. Both Phases of Fluorescence Decay Reflect Internalization and Subsequent Acidification of Reporters from Surface Membrane

(A) Time course of normalized fluorescence intensity change in small region (red, 1.6μm diameter, n = 41 traces) and larger region (green, 3.5μm diameter, n = 41 traces) after single vesicle fusion.

(B) Averaged single vesicle fluorescence intensity as a function of time in the presence of bafilomycin (filled black circle, n = 92 traces), as well as in the absence of bafilomycin (open gray circle, n= 68 traces).

(C) Fluorescence intensity of synaptic boutons before (pH=7.3) and after (pH=5.6) extracellular acidification (right panel, n = 155 traces), with synapses expressing a new pH sensor with phluorin fused to the cytoplasmic C-terminal of Synaptophysin (left panel).
(D) Fluorescence intensity as a function of time with extracellular pH alternating between 7.3 and 5.6 before and after exocytosis of a population of vesicles (right panel, n = 45 traces), when SypHluorin 4x (left panel) are expressed in synapses.
Error bars represent SEM

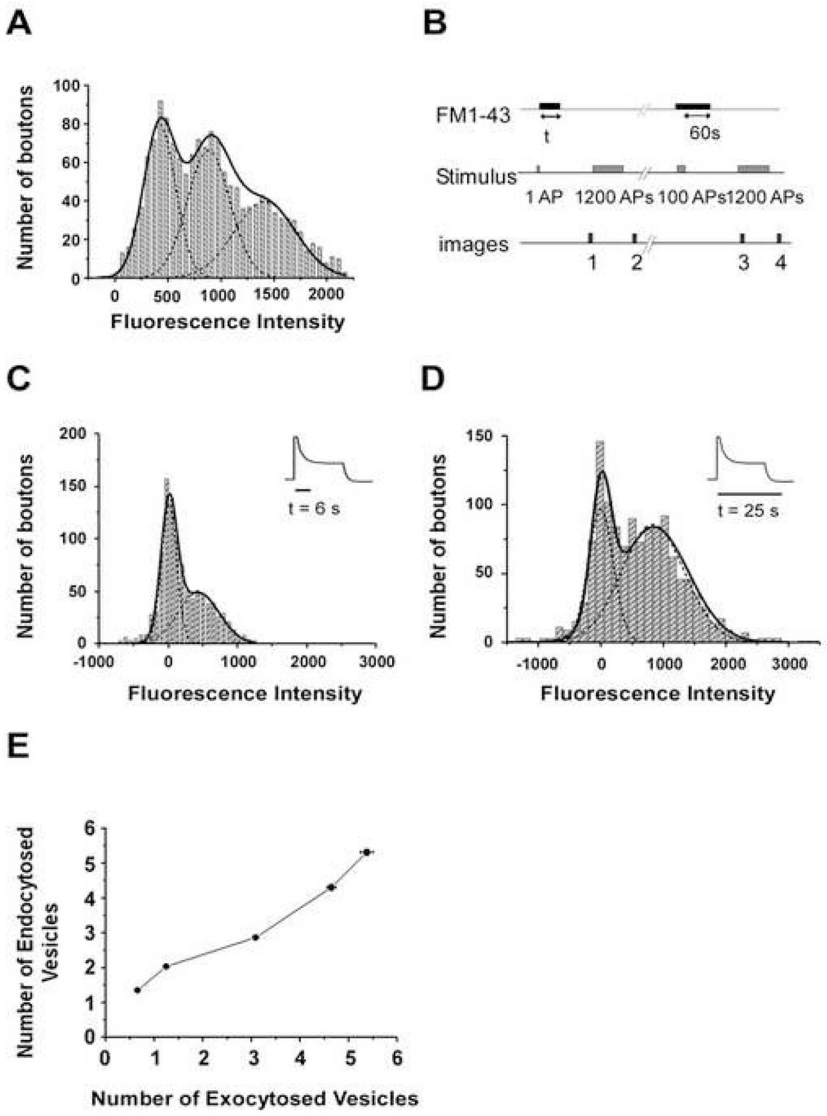

Figure 4. Two Distinct Vesicles Internalized After One Vesicle Fusion

(A) Estimation of fluorescence intensity of a single vesicle labeled with FM 1-43. The solid and dashed lines are the overall and individual fits to multiple Gaussians ($P = 0.99$, χ^2 test, d.f. = 40). The distribution of fluorescence has peaks at integral multiples of quantized fluorescence intensity. The average distance between the peaks was 451 units and is taken to correspond to the fluorescence of a single vesicle.

(B) Protocol used to measure the FM 1-43 uptake at individual synapse during a designated time of dye exposure (t) after single action potential. The fluorescence loss between images 1 and 2 provided the measurement of FM uptake by single action potential at individual synapses. The subtraction image of images 3 and 4 provided the identification of functional synapses. The positions of functional synapses were retrospectively projected onto the subtraction image of images 1 and 2, and the total fluorescence intensity of each functional synapse was measured. The stimulation frequency was 10Hz for 1200 action potentials, and 20Hz for 100 action potentials.

(C) Distribution of fluorescence intensity at individual synapses after labeling the internalized vesicles by the end of the ‘initial state’. Insert presents the time of FM 1-43

exposure corresponding to SypHluorin response. The solid and dashed lines are the overall and individual fits to multiple Gaussians, showing peaks at 11 and 435 ($P = 0.99$, χ^2 test, d.f. = 30).

(D) Distribution of fluorescence intensity at individual synapses after labeling the internalized vesicles by the end the 'plateau state'. Insert presents the time of FM 1-43 exposure corresponding to SypHluorin response. The solid and dashed lines are the overall and individual fits to multiple Gaussians, showing peaks at 0 and 850 ($P = 0.96$, χ^2 test, d.f. = 39).

(E) A plot of endocytosed vesicle number (estimated by FM 1-43 uptake during 35s) as a function of exocytosed vesicle number (estimated by SypHluorin response) under the stimulation of 2, 5, 10, 20, and 30 action potentials at 20Hz. The vesicle number was calculated by: $F_{total}/F_{single\ vesicle,}$ where F_{total} is the total fluorescence intensity, and $F_{single\ vesicle}$ is the fluorescence intensity of single vesicle. Error bars represent SEM

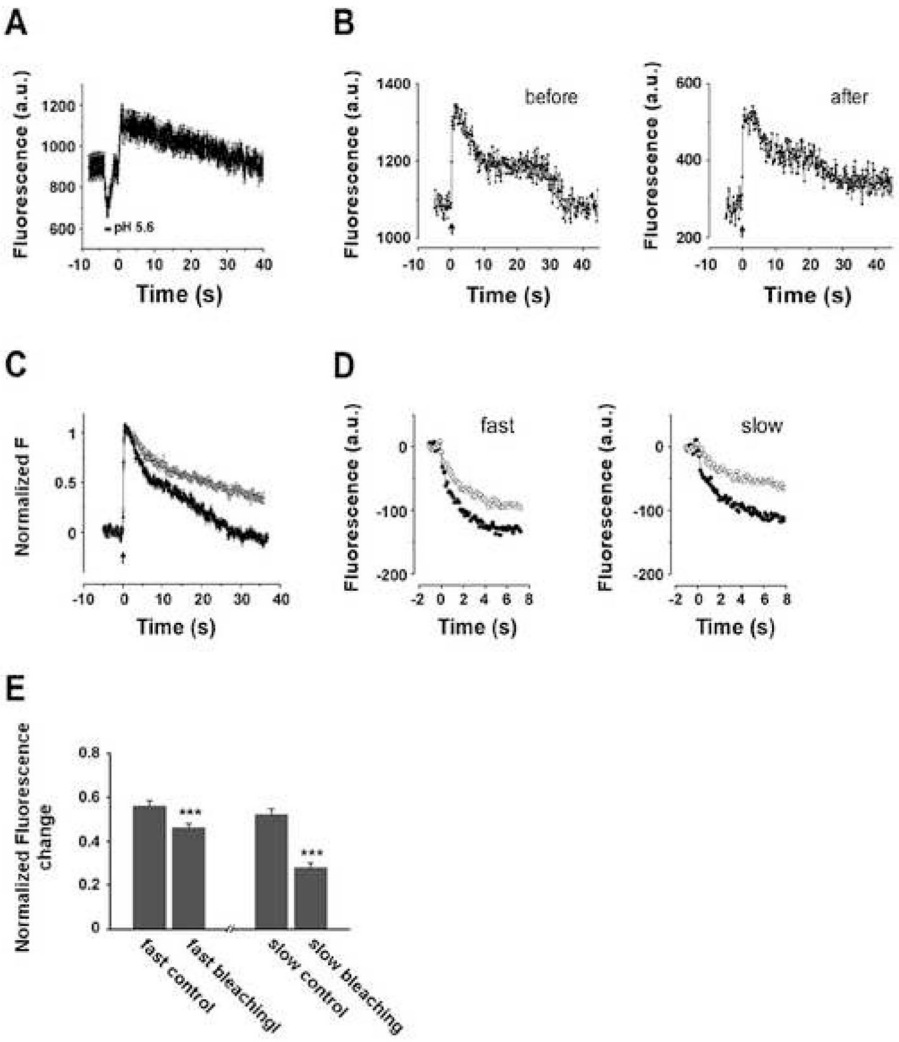

Figure 5. Newly Exocytosed SypHluorins were Preferentially Retrieved in Both Endocytosis

(A) Estimation of the amount of SypHluorins on the bouton surface at rest. A pulse of an acidic solution (pH 5.6) was applied before the single vesicle fusion being evoked at 0s. Averaging over 47 responses shows that the amount of SypHluorins on surface is about 93% of that inside a single vesicle.

(B) Example traces of single vesicle response before (left panel) and after photobleaching (right panel).

(C) Comparison of averaged fluorescence recovery after single vesicle fusion before (filled circle, n = 92 traces) and after photobleaching (open circle, n = 96 traces).

(D) Individual traces in C were realigned with the initial time of the fast endocytosis (left panel) or slow endocytosis (right panel), then averaged.

(E) Photobleaching surface SypHluorins reduces fluorescence intensity change in both the fast and slow endocytosis (See text). ***$p < 0.001$, paired t test.

Error bars represent SEM

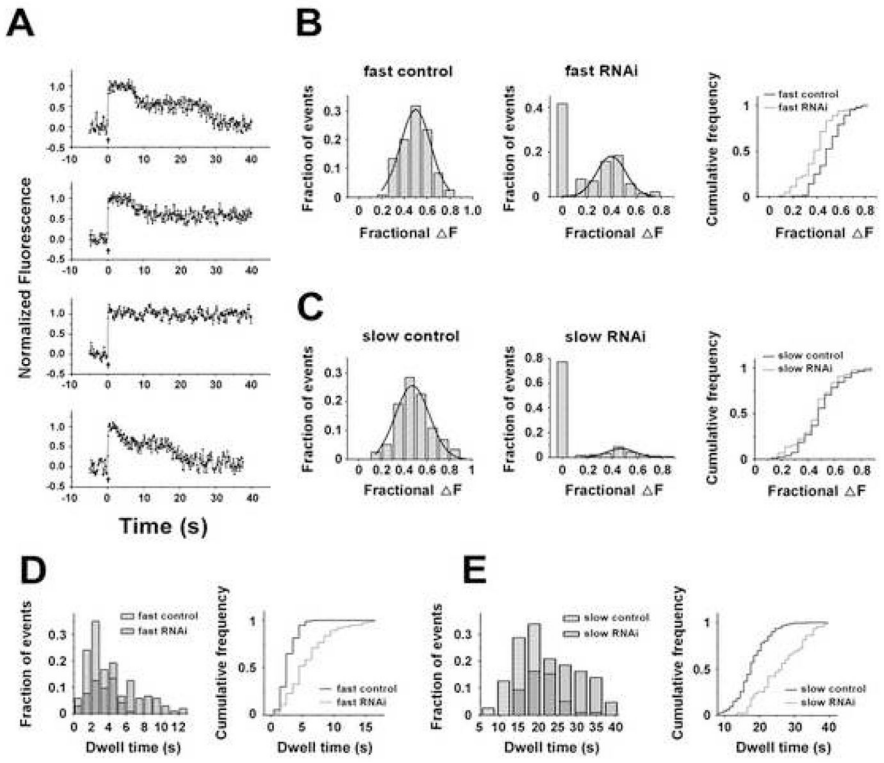

Figure 6. Clathrin Knockdown by RNAi Inhibits Both Endocytosis

(A) Example traces of single vesicle response with clathrin RNAi knockdown (upper 3 panels), and control (the bottom panel). The responses with clathrin RNAi knockdown can be classified into three groups. (i). Both the fast and slow endocytosis were detectable (accounting for ~20% of the total recordings), as shown in the top panel; (ii). Only the fast endocytosis was detected (~38% of the total recordings), as shown in the second panel; (iii). Neither fast nor slow endocytosis was detected (~42% of the total recordings), as shown in the third panel. Bottom panel presents an example trace of single vesicle response from a neuron transfected with scrambled RNAi (control).

(B and C) Clathrin RNAi knockdown inhibits both the fast (B) and slow (C) endocytosis. Frequency distribution of fractional fluorescence decrease during each endocytosis in control neurons (n=120 traces) is shown in the left panels, and in RNAi knockdown neurons (n =192 traces) is shown in the middle panels. The traces without detectable endocytosis were grouped as a bar at 0. The detectable endocytosis events were further fitted with Gaussian distribution (smooth curves). Right panels are cumulative histograms for events in control neurons and detectable events in RNAi knockdown neurons. Gaussian fits of the fast endocytosis in (B) yielded an estimation of 0.50 ± 0.11 (mean ± SD, n = 192 traces) for control and 0.40 ± 0.12 (mean ± SD, n = 104 traces) for the detectable events in CHC-RNAi knockdown. Two populations are significantly different, ***$p < 0.001$, t test. Gaussian fits of the slow endocytosis in (C) yielded estimations of 0.47 ± 0.14 (mean ± SD, n = 192 traces) for control and 0.47 ± 0.11 (mean ± SD, n = 43 traces) for the detectable events in RNAi knockdown. No significant difference was observed, $p > 0.05$, t test.

(D and E) Clathrin knockdown delays both endocytosis. Left panels in (D) and (E) present frequency dwell time distributions of the fast (D) and slow (E) endocytosis detected in RNAi knockdown neurons (filled gray bar, n = 104 traces for the fast endocytosis, n = 43 traces for the slow endocytosis) and control neurons (striped bar, n = 120 for both endocytosis). Right panels are the cumulative dwell time distributions of the fast (D) and

slow (E) endocytosis. For both endocytosis, clathrin knockdown significantly prolonged the dwell time (see text), ***$p < 0.001$, t test compared to control.

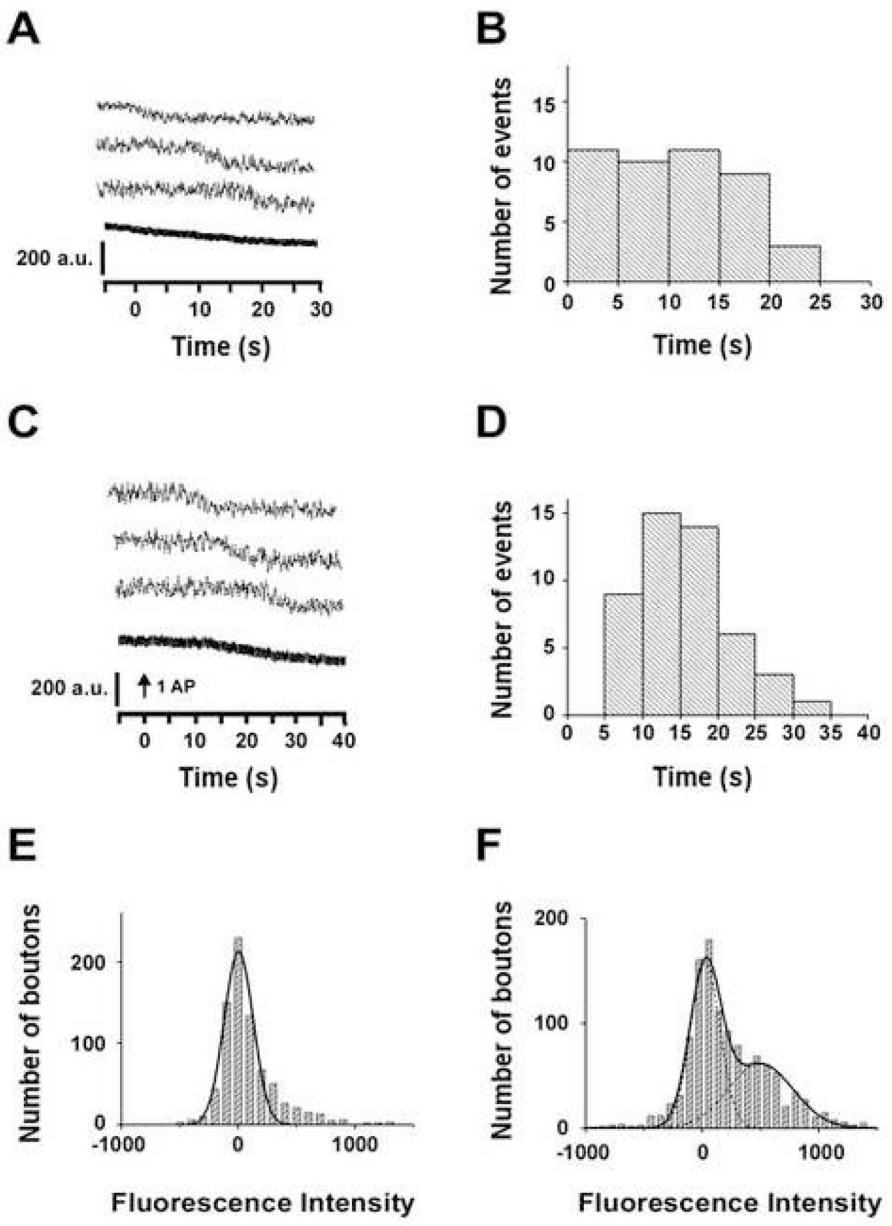

Figure 7. Spontaneous Endocytosis Detected by SypHluorins and FM 1-43

(A) Example traces of spontaneous vesicle retrieval observed from single bouton expressing SypHluorins in the absence of stimulation (upper three panels). The bottom panel shows the average trace over 146 boutons, including 53 boutons with retrieval events and 93 boutons without retrieval events.

(B) Distribution of the initial time for 53 retrieval events observed in A. The recording started from −5 sec and lasted for 30 sec.

(C) Example traces of vesicle retrieval observed from single bouton expressing SypHluorins with single stimulus, but without evoked exocytosis events (upper three panels). The bottom panel shows the average trace over 104 boutons, including 46 boutons with retrieval events and 58 boutons without retrieval events.

(D) Distribution of the initial time for 46 retrieval events observed in C. The recording started from −5 sec, the stimulus was delivered at 0 sec.

(E) Distribution of fluorescence intensity of FM 1-43 at individual synapses after exposing the neurons in 10 μM FM 1-43 for 6 sec without stimulation.
(F) As the same as E, but prolonging the dye exposure time to 25 sec. The solid and dashed lines in E and F are the overall and individual fits to single (E) or multiple Gaussians (F), showing single peak at 3 in E and multiple peaks at 2 and 475 in F.

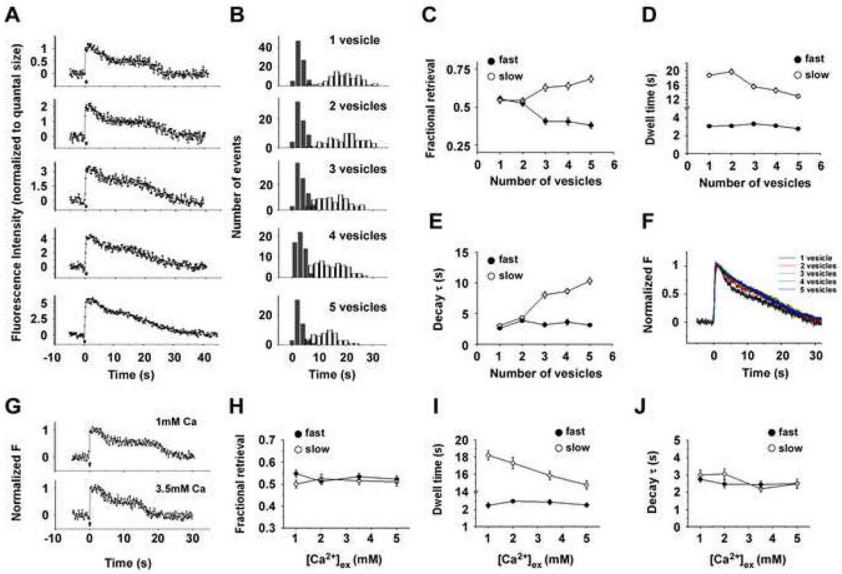

Figure 8. Increased Activity Selectively Accelerates the Slow Endocytosis, but Not the Fast Endocytosis

(A) Example traces of fluorescence intensity as a function of time following 1, 2, 3, 4, and 5 vesicle fusion events. Action Potentials (1Hz, 5Hz, 10Hz, 20Hz and 30Hz with duration of 0.5s) were delivered at 0s, as indicated by the bars.

(B) Comparisons of the dwell time distributions of endocytosis after different number of exocytosis events. Each histogram shows the dwell time distribution of the fast (filled bar) and slow (open bar) endocytosis after the release of one vesicle (n=86), two vesicles (n=64), three vesicles (n=64), four vesicles (n=51) and five vesicles (n=51). Further kinetic analyses of these traces are presented in C–F.

(C) Fractional retrieval of SypHluorins by the fast (filled circle) and slow (open circle) endocytosis as a function of the number of exocytosed vesicles. With the increased number of exocytosed vesicles, a larger fraction of SypHluorins was retrieved by the slow endocytosis.

(D) Averaged dwell time of the fast (filled circle) and slow (open circle) endocytosis as a function of the number of exocytosed vesicles. Increasing vesicle number shortened the dwell time of the slow endocytosis, but had no significant effect on the fast endocytosis.

(E) Averaged decay time constant of the fast (filled circle) and slow (open circle) endocytosis as a function of the number of exocytosed vesicles. Increasing vesicle number prolonged the decay time constant of the slow endocytosis, but not the fast endocytosis.

(F) Normalized average traces of fluorescence responses after multiple vesicle fusions. Single exponential fit provided a relatively good account of the fluorescence decay except for one vesicle, yielding time constant (τ) of 19.6 ± 0.7 s, 17.7 ± 1.4 s, 16.3 ± 0.9 s, 15.6 ± 1.0s and 14.4 ± 0.7 s for 1, 2, 3, 4, and 5 vesicles, respectively. No significant differences were observed between 2–5 vesicles (Turkey's multiple comparison test, $p>0.05$)

(G) Example traces of fluorescence intensity as a function of time for single vesicle fusion in 1mM and 3.5mM external calcium. Action Potential was delivered at 0s, as indicated by the arrow.

(H) Fractional retrieval of SypHluorins by the fast (filled circle) and slow (open circle) endocytosis as a function of $[Ca^{2+}]_{ex}$, after single vesicle fusion. The number of single vesicle fusion events for different $[Ca^{2+}]_{ex}$ are: n = 49 for 1mM, n = 44 for 2mM, n = 51 for 3.5mM, and n = 43 for 5mM. No significant differences were observed for both the fast and

slow endocytosis, with $[Ca^{2+}]_{ex}$ increased from 1mM to 5mM (Turkey's multiple comparison test, $p>0.05$). Further kinetic analyses of these traces are presented in I and J.
(I) Averaged dwell time of the fast (filled circle) and slow (open circle) endocytosis as a function of $[Ca^{2+}]_{ex}$, after single vesicle fusion. Increasing $[Ca2+]_{ex}$ shortened the dwell time of the slow endocytosis, but had no effect on the fast endocytosis. (Turkey's multiple comparison test, at the level of 0.05).
(J) Averaged decay time constant of the fast (filled circle) and slow (open circle) endocytosis as a function of $[Ca^{2+}]_{ex}$, after single vesicle fusion. No significant differences were observed for 1mM to 5mM for both endocytosis (Turkey's multiple comparison test, $p>0.05$).
Error bars represent SEM.

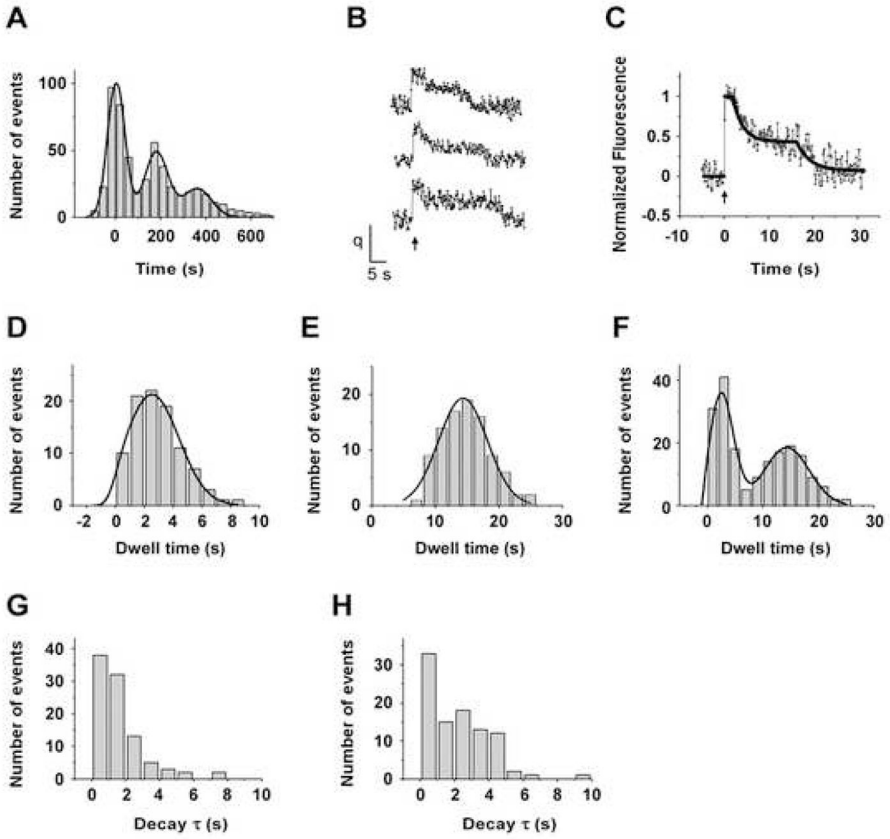

Figure 9. Two-phase of Endocytosis after Single Vesicle Fusion Detected by vGlut1-pHluorin

(A) Histogram of bouton fluorescence for 533 single stimulus presentations from 65 boutons. ($P = 0.99$, χ^2 test, d.f. = 21). Smooth solid curve is the sum of three Gaussian distributions expected for quantal releases, yielding a baseline noise standard deviation of 37.9 fluorescence units, and mean single vesicle fluorescence of 181.4 units with a standard deviation of 51.4 units. Thus, the signal to noise ratio for single vesicle detection is about 4.8 and the variability in expression of the reporter among vesicles is at most 28%.

(B) Example traces of fluorescence intensity as a function of time for single vesicles. Single action potential was delivered at 0s, as indicated by the arrow.

(C) An example fit (black line) of a trace with two distinct phases of exponential decay.

(D) Histogram of dwell time distribution of the fast endocytosis for 95 vesicles. Smooth curve is the fit with Gaussian distribution, yielding a mean of 2.5s with a standard deviation of 1.8s.

(E) Dwell time histogram of the slow endocytosis. Gaussian fit yielded a mean of 14.4s with a standard deviation of 3.8s.

(F) Distribution of combined dwell times of the fast and slow endocytosis. Smooth curve is the fit with two-component Gaussian distribution, yielding a mean of 2.5s with a standard deviation of 1.8s for the first component, and a mean of 14.7s with a standard deviation of 4.5s for the second component.

(G) Histogram of the reacidification time constant for the fast endocytosis, with a mean of 1.5 ± 0.2s.

(H) Histogram of the reacidification time constant for the slow endocytosis, with a mean of 2.2 ± 0.2s.

Data in (G) and (H) are presented as mean ± SEM

Table 1

Comparison of Sensor Performance in Cultured Hippocampal Neurons

	F0	ΔF	ΔF/F0	ΔF/F0½
Synaptophluorin	1 ± 0.04	1 ± 0.06	1 ± 0.05	1 ± 0.04
SypHluorin 1x	0.63 ± 0.02	1.21 ± 0.04	1.90 ± 0.10	1.52 ± 0.07
SypHluorin 2x	0.47 ± 0.02	2.01 ± 0.06	4.28 ± 0.20	2.93 ± 0.10
SypHluorin 4x	0.31 ± 0.02	1.74 ± 0.05	5.57 ± 0.30	3.12 ± 0.14

F0: fluorescence intensity of synapses before stimulation

ΔF: the peak change in fluorescence intensity upon stimulation

ΔF/F0: the signal-background ratio

ΔF/F01/2: the signal-noise ratio

Data are obtained from a stimulation with 40 action potentials at 20Hz, normalized to the corresponding value of Synaptophluorin, presented as mean ± SEM